Neuron, Vol. 44, 823–834, December 2, 2004, Copyright ©2004 by Cell Press

A Conserved Tripeptide in CNG and HCN Channels Regulates Ligand Gating by Controlling C-Terminal Oligomerization

Lei Zhou,[1] Nelson B. Olivier,[2] Huan Yao,[1] Edgar C. Young,[1] and Steven A. Siegelbaum[1,3,*]
[1]Center for Neurobiology and Behavior
[2]Department of Biochemistry and Molecular Biophysics
[3]Department of Pharmacology
Howard Hughes Medical Institute
Columbia University
722 West 168 Street
New York, New York 10032

Summary

Cyclic nucleotides directly enhance the opening of the tetrameric CNG and HCN channels, although the mechanism remains unclear. We examined why HCN and certain CNG subunits form functional homomeric channels, whereas other CNG subunits only function in heteromeric channels. The "defect" in the CNGA4 subunit that prevents its homomeric expression was localized to its C-linker, which connects the transmembrane domain to the binding domain and contains a tripeptide that decreases the efficacy of ligand gating. Remarkably, replacement of the homologous HCN tripeptide with the CNGA4 sequence transformed cAMP into an inverse agonist that inhibits HCN channel opening. Using analytical ultracentrifugation, we identified the structural basis for this gating switch: whereas cAMP normally enhances the assembly of HCN C-terminal domains into a tetrameric gating ring, inclusion of the CNGA4 tripeptide reversed this action so that cAMP now causes gating ring disassembly. Thus, ligand gating depends on the dynamic oligomerization of C-terminal binding domains.

Introduction

The ligand binding and regulatory domains of a large family of tetrameric ion channels can oligomerize into either a 2-fold symmetric dimer-of-dimers (Kuo et al., 2003; Schumacher et al., 2001; Sun et al., 2002; Zhou et al., 2004) or a 4-fold symmetric tetrameric gating ring (Jiang et al., 2002; Zagotta et al., 2003). However, it is unclear how these structures, determined by X-ray crystallography, function to regulate channel gating. Are such oligomers static, or are they dynamically controlled by ligand binding? And is the assembly or disassembly of such structures important in regulating channel opening and closing? Here, we address such questions for two related classes of tetrameric channels that are directly regulated by cyclic nucleotide binding, the cyclic nucleotide-gated channels (CNG) important for sensory signal transduction (Kaupp and Seifert, 2002; Matulef and Zagotta, 2003; Zagotta and Siegelbaum, 1996) and the hyperpolarization-activated cation channels (HCN) that control cardiac pacemaker activity and neuronal excitability (Robinson and Siegelbaum, 2003).

In vertebrates, there are six homologous CNG channel subunits. CNGA1 (Kaupp et al., 1989), CNGA2 (Dhallan et al., 1990), and CNGA3 (Weyand et al., 1994), referred to as α subunits, all form functional homomeric channels. In contrast, CNGA4 (Bradley et al., 1994; Liman and Buck, 1994), CNGB1 (Cheng et al., 2003), and CNGB3 (Gerstner et al., 2000), referred to as β subunits, fail to form functional homomers but coassemble with α subunits to form heteromers with novel properties. Native CNG channels are thought to be heterotetramers composed of two or three identical α subunits and one or more types of β subunits (Peng et al., 2004; Weitz et al., 2002; Zheng et al., 2002; Zheng and Zagotta, 2004; Zhong et al., 2002). At present, the factors that prevent functional expression remain unknown for any of the β subunits, although the cyclic nucleotide binding domain (CNBD) of the CNGA4 β subunit is clearly functional (Young et al., 2001). All four HCN subunits (HCN1–4) can form functional homomers and so act as α subunits; most of these subunits can also assemble with each other to form heteromers with novel properties that resemble hyperpolarization-activated channels in neurons (Chen et al., 2001; Ulens and Tytgat, 2001) and cardiac myocytes (Altomare et al., 2003; Much et al., 2003).

A recent X-ray crystal structure of cyclic nucleotide bound forms of a soluble C-terminal domain of HCN2, consisting of the CNBD and C-linker, has provided important insights into the mechanism of cyclic nucleotide gating (Zagotta et al., 2003). Four C-terminal domains are seen to assemble into a 4-fold symmetric gating ring in the presence of cAMP. Analytical ultracentrifugation studies of the oligomerization state of the soluble polypeptide in solution indicate that cAMP binding promotes assembly of the tetrameric gating ring; in the absence of cAMP, the polypeptides exist as dimers or monomers. Previous low-resolution structures (Higgins et al., 2002; Scott et al., 2001) and functional studies (Liu et al., 1998) of CNG channels suggested that the four subunits of a channel may assemble as a 2-fold symmetric dimer-of-dimers. Based on a functional analysis of the stoichiometry of cAMP gating of HCN channels, our laboratory suggested that channel gating by ligand may involve a transition from a 2-fold symmetric dimer-of-dimers to a 4-fold symmetric gating ring (Ulens and Siegelbaum, 2003). However, direct evidence as to whether gating ring assembly is indeed important for channel activation is lacking.

Here, we address the mechanism of cyclic nucleotide gating in both CNG and HCN channels by first demonstrating that the C-linker of the CNGA4 β subunit is responsible for its lack of functional expression. We next identify a tripeptide near the N terminus of the C-linker, which is conserved among CNG α subunits and HCN subunits but divergent in CNG β subunits, that exerts a profound effect on ligand gating. Whereas the tripeptide of CNG α subunits and HCN subunits promotes a high efficacy of ligand gating, the CNGA4 tripeptide dramatically decreases ligand efficacy. When the HCN tripep-

*Correspondence: sas8@columbia.edu

tide is replaced with the CNGA4 tripeptide, the polarity of action of cyclic nucleotide binding on both channel gating and oligomerization of the C-terminal polypeptide is reversed. In the mutant, cAMP binding inhibits channel opening and favors the disassembly of C-terminal tetramers into dimers. These results thus provide strong evidence that the assembly of the 4-fold symmetric cytoplasmic gating ring from a dimer-of-dimers is a key event in the coupling of ligand binding to channel opening.

Results

The fCNGA4 β Subunit C-Linker Prevents Expression of Functional Homomeric Channels

We first examined why CNG α subunits form functional homotetrameric channels, whereas the CNGA4 β subunit does not. We initially characterized the properties of a CNGA4 subunit that we cloned from catfish olfactory epithelium (fCNGA4) that is 54% identical to rat CNGA4 (Bradley et al., 1994; Liman and Buck, 1994) (see Supplemental Figure S1 at http://www.neuron.org/cgi/content/full/44/5/823/DC1/). When expressed alone in *Xenopus* oocytes, fCNGA4 failed to yield detectable cyclic nucleotide-gated current (Figure 1A). However, coexpression of this subunit with either the catfish olfactory α subunit (fCNGA2) or a highly expressing α subunit chimera (ROONS) (see Experimental Procedures; Goulding et al., 1994; Tibbs et al., 1997, 1998) generated heteromers with novel properties, similar to results with rat CNGA4 (Bradley et al., 1994; Liman and Buck, 1994) (Figure 1A). Thus, fCNGA2 + fCNGA4 heteromers exhibited a high sensitivity to cAMP, with a $K_{1/2}$ (2.3 ± 0.5 μM) similar to that of native catfish CNG channels (Goulding et al., 1992) but much lower than that of fCNGA2 homomers (97.7 ± 12.6 μM). Similarly, fCNGA4 + ROONS channels also had a much higher sensitivity to cAMP (4.3 ± 0.7 μM) compared to ROONS homomers (320 ± 56.9 μM) (Figure 1C).

A second difference between α subunit homomeric channels and channels that incorporate fCNGA4 was that the heteromers exhibited a marked outward current rectification, similar to previous results for other heteromeric CNG channels (Bonigk et al., 1999; Bradley et al., 1994; Liman and Buck, 1994). Thus, fCNGA4-containing heteromers generated macroscopic currents whose absolute value was more than 5-fold larger at +100 mV than at −100 mV (I_{+100}/I_{-100} = 5.5 ± 0.6; n = 7; Figure 2B). This rectification was largely due to voltage-dependent gating, since the instantaneous current rectification through open heteromeric channels was small (I_{+100}/I_{-100} = 1.4 ± 0.2; n = 8). In contrast, the steady-state rectification of ROONS homomers was small and equivalent to the instantaneous current rectification through the open channel (I_{+100}/I_{-100} = 1.31 ± 0.03; n = 3).

A third difference is that the openings of α subunit homomeric channels were well resolved, whereas α + fCNGA4 heteromers exhibited flickery single-channel openings (see Supplemental Figure S2 at http://www.neuron.org/cgi/content/full/44/5/823/DC1/), similar to the flickery openings of native CNG channels (Bonigk et al., 1999; Bucossi et al., 1997; Karpen, 1997). These results show that fCNGA4 acts as a typical CNG β subunit: it failed to form functional homomeric channels but coassembled with α subunits to modify gating in a stereotypical pattern.

Which region of fCNGA4 prevents it from forming functional homomers? By constructing a large series of chimeras between CNG α subunits and fCNGA4, we found that replacement of the first 78 out of 86 residues of the C-linker (L) of fCNGA4 with the corresponding residues of CNGA1 was both necessary and sufficient to yield a chimeric subunit (see Figure 2A) that generated functional homomeric channels with large CNG currents (Figure 1A). The channels formed from this "rescued" subunit, β-α(L_{1-78}), had a high sensitivity to cAMP ($K_{1/2}$ = 5.2 ± 1.0 μM) and cGMP ($K_{1/2}$ = 3.4 ± 0.3 μM), similar to native fish CNG channels (Goulding et al., 1992) and α + β heteromers, but in contrast to the low agonist sensitivity of fCNGA2 homomers (Figure 1C). The rescued β subunit also exhibited rapidly flickering single-channel currents, similar to those of ROONS + fCNGA4 heteromers (see Supplemental Figure S2 at http://www.neuron.org/cgi/content/full/44/5/823/DC1/). However, β-α(L_{1-78}) homomeric channels displayed two properties distinct from α + β heteromers. First, their dose-response curves for both cAMP and cGMP were steeper than those of α + β heteromers. Second, β-α(L_{1-78}) channels showed very little outward rectification, at either saturating or subsaturating concentrations of ligand (Figure 1B).

The C-Linker of the fCNGA4 β Subunit Contains a Tripeptide that Suppresses the Efficacy of Cyclic Nucleotide Gating

What is the mechanism by which the β subunit C-linker prevents the expression of functional homomeric channels? Previous studies have shown that sulfhydryl oxidizing agents, but not cyclic nucleotides, are capable of activating current through rat CNGA4 homomers, indicating that assembled CNGA4 channels can traffic to the membrane but cannot be gated by cyclic nucleotide (Broillet and Firestein, 1997). In support of a defect in ligand gating, we found that fCNGA4 subunits could coassemble and traffic to the surface membrane when expressed alone (based on biochemical and fluorescence data; L.Z. and S.A.S., unpublished data). To examine a possible effect of the β subunit C-linker on cyclic nucleotide gating, we used a strategy in which α subunits were coexpressed with either a wild-type β subunit or a chimeric β subunit whose C-linker was partially replaced by α subunit sequence. We reasoned that any difference in channel properties between two such pairs of heteromers must reflect differences between the function of the β subunit C-linker sequence and the substituted α subunit sequence, the only structural differences between the two channels.

We first examined a chimeric fCNGA4 β subunit whose first 54 C-linker residues, the L1 region (Paoletti et al., 1999), were replaced with CNGA1 α subunit sequence [β-α(L_{1-54}); see icon in Figure 2B]. β-α(L_{1-54}) had an advantage over β-α(L_{1-78}) in these experiments, because the former subunit expressed only very small homomeric CNG currents (<10 pA), minimizing the extent to which homomeric currents could contaminate currents from the heteromers of interest.

Coexpression of β-α(L_{1-54}) with ROONS α subunits yielded large CNG currents with a much higher sensitiv-

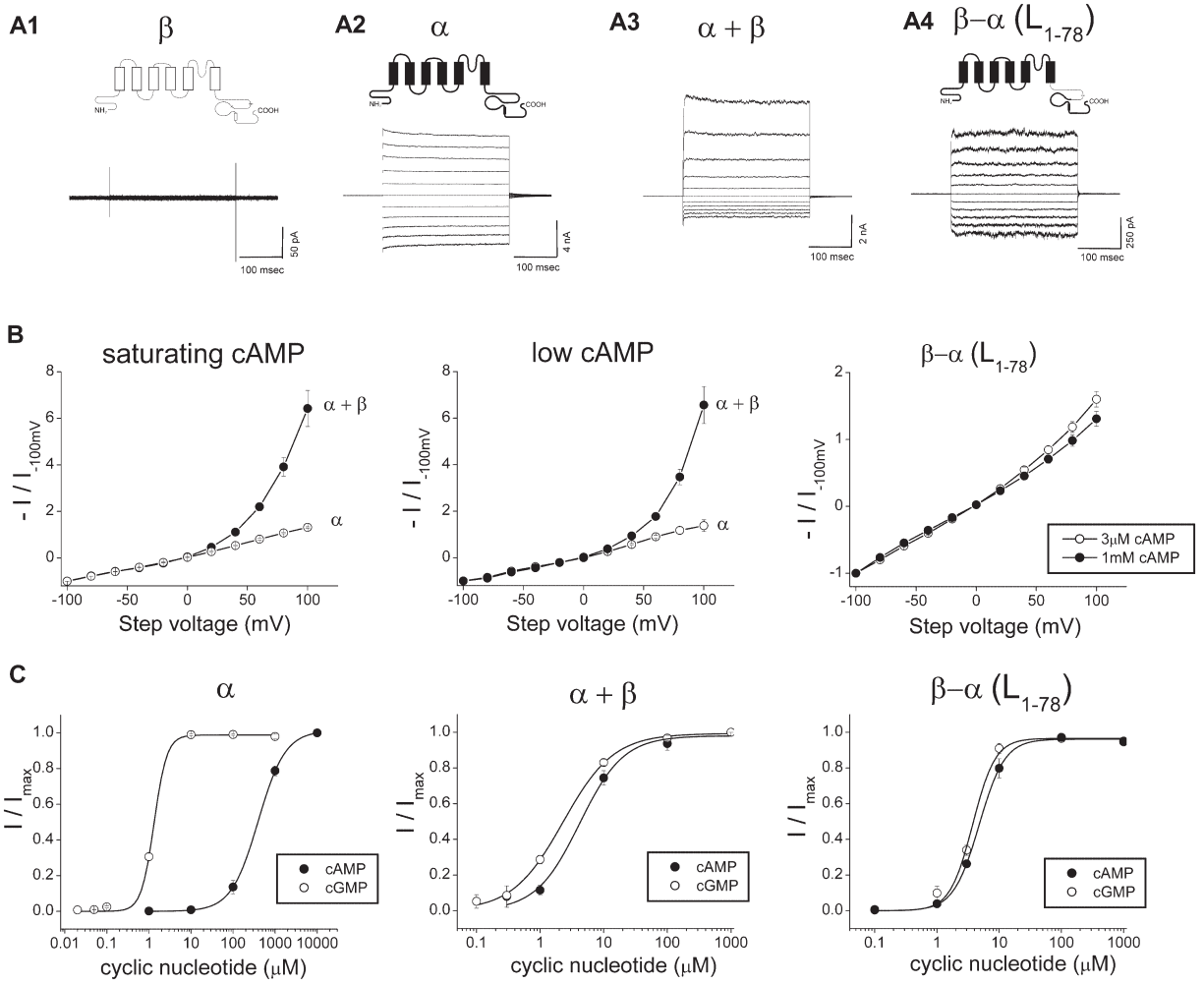

Figure 1. Comparison of Properties of CNG α Subunit Homomers, α + β Subunit Heteromers, and Rescued β Subunit Homomers

(A) Currents elicited by cyclic nucleotide in inside-out patches from oocytes expressing the following: A1, a CNG channel β subunit (fish CNGA4) alone; A2, an α subunit (ROONS) alone; A3, both α + β subunits (ROONS + fCNGA4); and A4, a rescued β subunit, β-α(L_{1-78}). Currents obtained in response to a series of voltage steps from −100 to +100 mV, in 20 mV intervals. Saturating concentrations of cAMP were applied for all recordings [10 mM for β and α subunits; 1 mM for α + β heteromers and β-α(L_{1-78})]. Icons show fCNGA4 β subunit sequence as thin lines and open rectangles and ROONS α subunit sequence as thick lines and filled rectangles.

(B) Current-voltage (I-V) curves for α subunit homomers, α + β heteromers, and rescued β-α(L_{1-78}) homomers. Steady-state CNG currents normalized to the absolute value of currents at −100 mV. The following concentrations of cAMP were used: α subunit homomers, 10 mM (saturating) and 100 μM (low); α + β heteromers, 1 mM (saturating) and 1 μM (low).

(C) Dose-response curves for α subunit homomers, α + β heteromers, and β-α(L_{1-78}) homomers. Mean $K_{1/2}$ (μM) and Hill coefficient (h) values (±SEM) with cGMP and cAMP obtained from fits of Hill equation are as follows. For α subunit (ROONS) homomers: cGMP, $K_{1/2}$ = 2.15 ± 0.24 and h = 1.68 ± 0.08 (n = 6); cAMP, $K_{1/2}$ = 320.4 ± 56.9 and h = 2.33 ± 0.40 (n = 7). For α + β heteromers: cGMP, $K_{1/2}$ = 2.33 ± 0.21 and h = 1.09 ± 0.07 (n = 5); cAMP, $K_{1/2}$ = 4.27 ± 0.68 and h = 1.28 ± 0.13 (n = 3). For β-α(L_{1-78}) homomers: cGMP, $K_{1/2}$ = 3.45 ± 0.35 and h = 2.46 ± 0.30 (n = 6); cAMP, $K_{1/2}$ = 5.16 ± 1.01 and h = 2.29 ± 0.14 (n = 7). All dose-response curves were measured at +80 mV.

ity to cAMP ($K_{1/2}$ of 6.9 ± 1.5 μM) than that of ROONS homomers, indicating efficient heteromer formation. Surprisingly, ROONS + β-α(L_{1-54}) heteromers showed a novel property compared to ROONS homomers or to ROONS + wild-type fCNGA4 heteromers: the extent of outward rectification was dependent on the cyclic nucleotide concentration. Thus, ROONS + β-α(L_{1-54}) heteromers exhibited little voltage-dependent gating with saturating concentrations of cAMP (I_{+80}/I_{-80} = 1.23 ± 0.02), whereas gating was significantly enhanced by depolarization at low concentrations of cAMP (I_{+80}/I_{-80} = 2.9 ± 0.28; Figure 2B).

By analyzing a series of C-linker chimeras, we found a tripeptide near the amino terminus of the C-linker (C-linker residues 11–13) that was responsible for this novel cAMP dependence of voltage gating (Figure 2C). In fCNGA4, the tripeptide sequence is FPN, whereas in CNGA1 it is QAR. When we coexpressed with ROONS the chimera in which the fCNGA4 tripeptide was replaced by the CNGA1 tripeptide (chimera β/QAR), the heteromeric channels displayed a much greater voltage dependence of gating at low cAMP (I_{+80}/I_{-80} = 3.71 ± 0.51) than at saturating cAMP (I_{+80}/I_{-80} = 1.42 ± 0.12). These channels also had a much higher sensitivity to

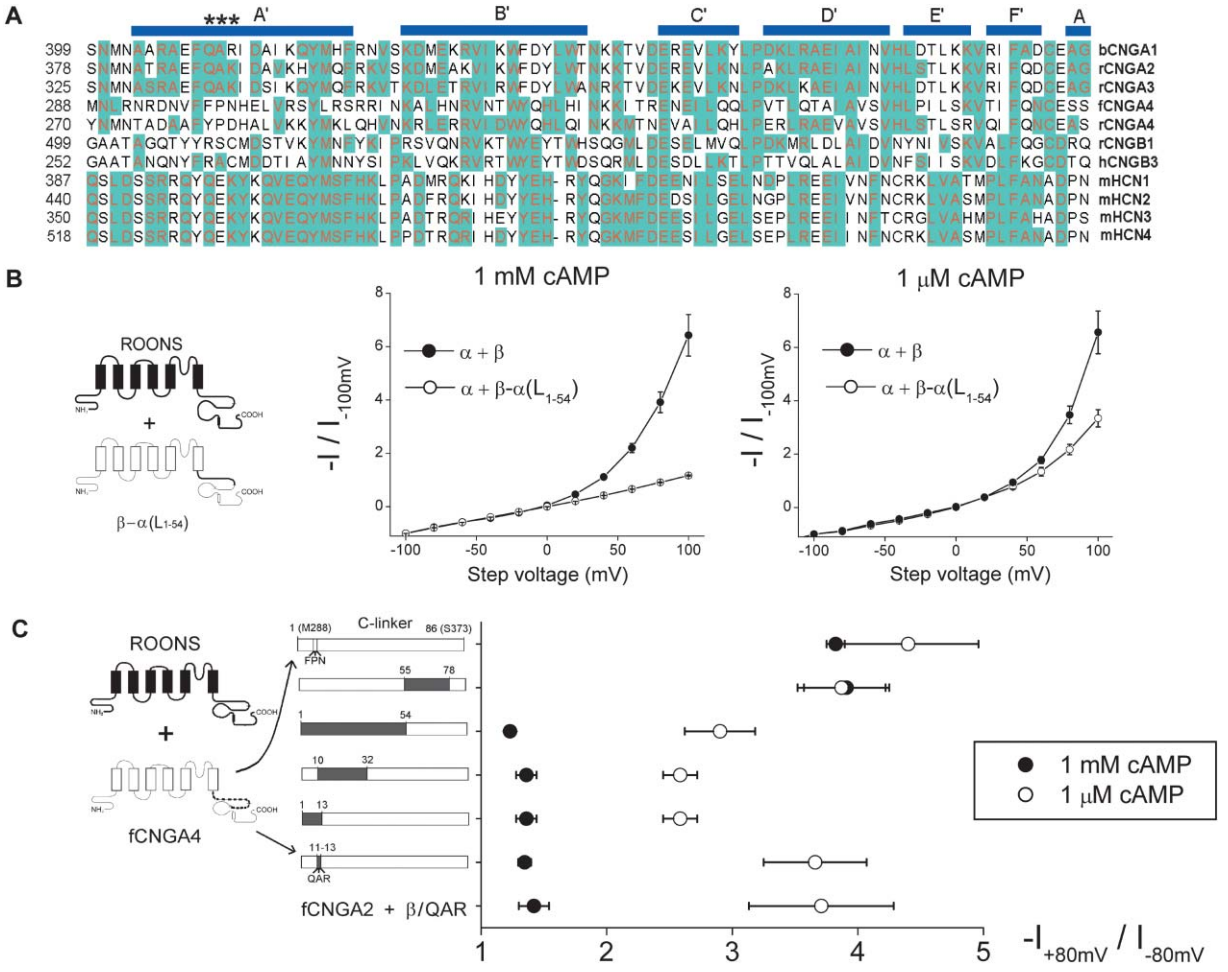

Figure 2. Identification of a Tripeptide Sequence Difference in the C-Linkers of α and β Subunits Responsible for the Dependence of Voltage Gating on Cyclic Nucleotide Concentration

(A) Sequence alignment of C-linker sequences from CNG and HCN channels. Starting amino acid numbers of C-linkers given at left (which correspond to C-linker residue 1). Bars show location of α helices in the X-ray crystal structure of a soluble C-terminal domain of HCN2 (C-linker + CNBD) with cAMP bound (Zagotta et al., 2003). Helices A′–F′ are in the C-linker; helix A is at the start of CNBD. Asterisks denote tripeptide sequence important for gating.

(B) Current-voltage relations for β-α(L_{1-54}) + ROONS heteromers show voltage-dependent gating at low concentrations of cAMP (right panel) but not at saturating cAMP (left panel). Icons on the left show the construction of β-α(L_{1-54}) (α subunit sequence, filled rectangles and thick lines; β subunit sequence, open rectangles and thin lines). I-V data for ROONS + fCNGA4 heteromers (α + β, filled circles) are shown for comparison. $K_{1/2}$ (μM) and Hill coefficients (h) for β-α(L_{1-54}) + ROONS heteromers were as follows: cAMP, $K_{1/2} = 6.9 \pm 1.5$ and $h = 1.18 \pm 0.13$ ($n = 4$); cGMP, $K_{1/2} = 0.74 \pm 0.05$ and $h = 2.85 \pm 0.07$ ($n = 4$).

(C) Voltage sensitivity of heteromeric channel currents generated by coexpressing ROONS plus various fCNGA4 C-linker chimeras. Ratio of steady-state current absolute values at +80 to −80 mV is plotted for saturating (1 mM, filled circles) or subsaturating (1 μM, open circles) cAMP. Horizontal bars to left of graph show the composition of the C-linker regions of the fCNGA4/α chimeras. Black areas indicate region of C-linker sequence of fCNGA4 that was replaced by CNGA1 α sequence. Numbers above rectangles show amino acid boundaries of C-linker chimeras, with 1 corresponding to the first C-linker residue of fCNGA4 (M288). Top row, data for ROONS (α) plus wild-type fCNGA4 (β). Bottom row, data for heteromer formed by coexpressing the fCNGA2 (α) together with the β/QAR chimera (see text).

cAMP ($K_{1/2} = 2.48 \pm 0.52$ μM; $n = 5$) than ROONS homomers, indicating efficient heteromer formation. Similar effects were observed when β/QAR was coexpressed with fCNGA2. No single or double point mutant chimeras fully reproduced the phenotype of the FPN to QAR triple mutation. A converse chimera in which QAR of ROONS was replaced by FPN failed to yield detectable CNG currents.

Why does the voltage dependence of gating depend on cAMP concentration? We hypothesized that replacement of the FPN tripeptide of fCNGA4 with the QAR tripeptide greatly enhanced the efficacy of ligand gating so that the maximal open probability of ROONS + β-α(L_{1-54}) or ROONS + β/QAR channels at saturating cAMP (P_{max}) approached one, even at negative voltages. As a result, depolarization could only enhance CNG current with subsaturating [cAMP], where open probability started out low at negative potentials. This hypothesis is consistent with previous results showing that the C-linker region of α subunits regulates the efficacy of ligand gating (Johnson and Zagotta, 2001; Paoletti et al., 1999; Zong et al., 1998) and previous results on the effects of cGMP concentration on the voltage dependence of rod CNG channels (Karpen et al., 1988).

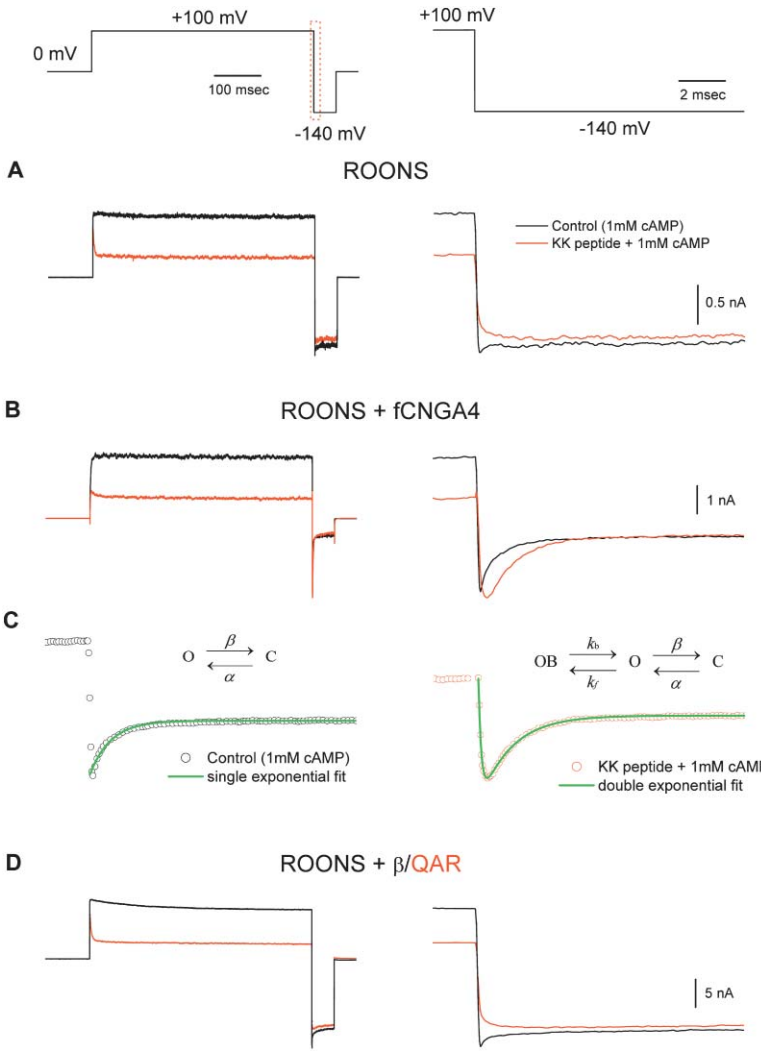

Figure 3. Tail Currents Generated upon Relief of Open-Channel Block Due to Hyperpolarization Reveals Effect of FPN Sequence to Decrease P_{max}

Macroscopic currents were recorded with 1 mM cAMP. Voltage protocol is shown at top. The time period around the voltage step from +100 mV to −140 mV (dotted rectangular box) is shown on an expanded timescale at right. Black traces, control current before KK peptide application; red traces, current in the presence of 10 μM KK peptide. (A) Currents from α subunit homomers (ROONS) in absence and presence of KK peptide. Note lack of tail currents with saturating concentrations of cyclic nucleotide (1 mM cAMP) in absence or presence of KK peptide, indicating $P_{max} \approx 1$. (B) Currents from ROONS + wild-type fCNGA4 heteromers under same conditions. Note a prominent tail current is seen upon step to −140 mV in absence of KK peptide (black trace), which reflects the inherent voltage dependence of gating. A larger and slower tail in the presence of KK peptide (red trace) reflects the rapid unblock and subsequent slow closing of channels driven into the open-blocked state during depolarization. (C) Circles show a further expanded view of current traces from (B) in absence (left) or presence (right) of KK peptide. Solid lines show best fit of two-state model in absence of KK peptide (left) or three-state model in presence of KK peptide (right) (see Experimental Procedures). Average calculated K_d for KK peptide was 2.6 ± 0.5 μM (n = 7) at +140 mV and 14.0 ± 1.7 μM at −140 mV (n = 9). The fits yielded the following mean rate constants at −140 mV (n = 8): β, 1327 ± 176 s^{-1}; α, 198 ± 30 s^{-1}; k_f, 3.25 ± 0.46 × 10^8 $M^{-1}s^{-1}$; k_b, 4391 ± 665 s^{-1}; P_{max}, 0.13 ± 0.02. (D) Tail currents are abolished in ROONS + β/QAR heteromers, indicating that $P_{max} \approx 1$.

The flickery single-channel currents of the heteromers prevented us from directly measuring P_{max}. We therefore measured P_{max} from the ratio of I_{max}, the maximal current elicited by saturating cyclic nucleotide at a negative holding voltage, to I_{total}, the current at the same voltage when all channels in the patch were forced open. I_{total} was determined by a strategy in which a voltage-dependent open-channel blocker was used to lock CNG channels in the open-blocked state (Figure 3). This blocker, a variant of the Shaker K^+ channel N-terminal "ball peptide" (KK peptide; Murrell-Lagnado and Aldrich, 1993), was previously shown to interact with CNG channels according to the following scheme: C ↔ O + B ↔ OB, where C is the closed state, O is the open state, B is blocker, and OB is the open-blocked state. Importantly, the affinity of the open state for blocker is greatly enhanced by depolarization (Kramer et al., 1994). Thus, application of a large positive voltage step in the presence of cyclic nucleotide and ball peptide will drive nearly all channels into the open-blocked state, even if initial open probability is low. As a result, when the membrane is stepped back to a negative voltage, a large tail current will be generated as the KK peptide rapidly dissociates (OB → O). The amplitude of the peak tail current provides an estimate of I_{total}.

ROONS homomers generated currents in saturating cAMP that were blocked by KK peptide at +100 mV but showed no prominent tail current when the membrane was stepped to −140 mV, consistent with single-channel results that P_{max} for ROONS is close to one (Figure 3A). In contrast, ROONS + fCNGA4 channels displayed a large tail current at −140 mV, whose peak amplitude was ~5-fold larger than the steady-state current at this voltage in the absence of KK peptide, indicating a P_{max} of ~0.2 (Figure 3B). Because some open channels will close before all channels unblock, the peak tail current provides a lower limit for I_{total}. Using a simple open-blocked model to correct for this effect (see Experimental Procedures), we estimate that the true P_{max} was ~0.1 (Figure 3C). In contrast to the large tail current with ROONS + fCNGA4 heteromers, ROONS + β/QAR channels displayed little tail current, indicating a high P_{max} (Figure 3D). ROONS + β-α(L_{1-54}) heteromers also had a high P_{max}, based on their lack of tail current (data not shown).

The FPN Tripeptide Reverses the Polarity of Ligand Gating in HCN Channels

How does the FPN sequence suppress the efficacy of ligand gating? According to allosteric models of channel

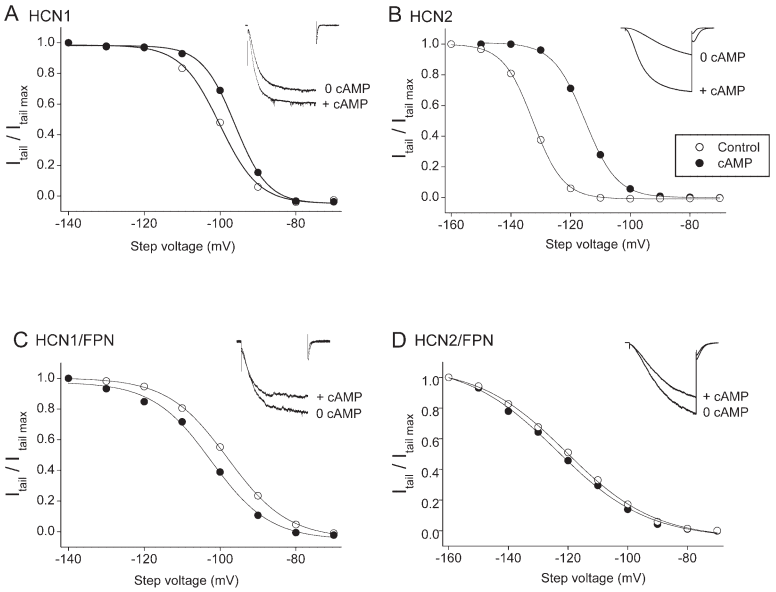

Figure 4. Mutating the QEK Tripeptide in the C-Linker of HCN1 and HCN2 to Homologous FPN Sequence from fCNGA4 Converts cAMP from an Agonist that Facilitates Voltage Gating into an Inverse Agonist that Inhibits Voltage Gating

(A and B) Individual tail current activation curves for wild-type HCN1 (A) or HCN2 (B) in absence (open circles) or presence (filled circles) of 10 μM cAMP. Curves plot fractional channel activation as a function of voltage during 3 s long hyperpolarizations. Superimposed curves show fits of Boltzmann equation. Insets compare HCN currents in absence (0 cAMP) and presence (+cAMP) of cAMP during hyperpolarizations to −110 mV (A) or −130 mV (B).

(C and D) Tail current activation curves for HCN1/FPN (C) and HCN2/FPN (D) in absence (open circles) or presence (filled circles) of 10 μM cAMP. Insets show effects of cAMP on currents in response to steps to −100 mV (C) or −120 mV (D). Basal $V_{1/2}$ values in the absence of cAMP: wild-type HCN1, mean $V_{1/2} = -103.6 \pm 1.5$ mV (n = 9); HCN1/FPN, $V_{1/2} = -99.8 \pm 1.0$ mV (n = 24; p = 0.059); wild-type HCN2, $V_{1/2} = -130.1 \pm 0.8$ mV (n = 10); HCN2/FPN, $V_{1/2} = -119.0 \pm 2.2$ mV (n = 16; $p < 0.001$).

gating, the FPN sequence could act by decreasing the efficiency with which the free energy available from ligand binding is coupled to enhance gating. Alternatively, it could make the inherent free energy change associated with channel opening in the absence of ligand even more unfavorable (Tibbs et al., 1997). Such questions cannot be readily addressed in CNG channels, where the effect of the FPN sequence can only be studied in the context of heteromeric channels. However, we found that the QAR tripeptide of CNGA1 is partially conserved as a QXK/R consensus motif in the C-linkers of the mammalian HCN channels, as well as in all other CNG α subunits (Figure 2A). We therefore examined the effect of the FPN sequence in the background of HCN channels, which offer an experimental advantage over CNG channels because they are activated by hyperpolarization in the absence of cyclic nucleotide. Thus, the effect of the FPN sequence on the inherent energetics of channel opening can be directly determined by its effect on the basal voltage dependence of gating. Effects of the FPN sequence on the coupling of ligand binding to channel opening can be separately measured by looking for changes in the actions of cAMP on HCN gating.

We examined two chimeras in which the QEK sequence of HCN1 and HCN2 was replaced by FPN (Figure 4). Both the HCN2/FPN and HCN1/FPN chimeras yielded functional channels that showed relatively normal activation in response to hyperpolarization in the absence of cAMP. Indeed, the chimeras showed a midpoint voltage of activation ($V_{1/2}$) in the absence of cAMP that was shifted to slightly more positive potentials compared to the wild-type subunits (Figure 4). This shows that the FPN mutation did not, in fact, make the intrinsic energetic cost of opening of HCN channels less favorable but rather had a small facilitatory effect. However, to our surprise, when we examined the effect of cAMP on these chimeras, we found that the FPN substitution converted cAMP from an agonist that facilitated channel opening into an inverse agonist that inhibited channel opening.

In wild-type HCN channels, cAMP enhanced gating by shifting activation to more positive potentials. At saturating concentrations of cAMP, the maximal depolarizing shift in $V_{1/2}$ (ΔV_{max}) for HCN1 was $+4.8 \pm 0.6$ mV (n = 9) (Figure 4A); for HCN2, the shift was 3-fold greater ($+16.5 \pm 0.7$ mV; n = 10) (Figure 4B). In contrast, cAMP binding caused a small but significant *hyperpolarizing* shift for both HCN1/FPN (Figure 4C) and HCN2/FPN channels (Figure 4D). Now ΔV_{max} was -3.1 ± 0.3 mV for HCN1/FPN (n = 24) and -1.7 ± 0.7 mV (n = 16) for HCN2.

The inhibitory effects, although small, were genuine: they were rapid, readily reversible, and highly reproducible (Figure 5A). Moreover, we found that the inhibitory responses were mediated by cAMP binding to the canonical CNBD, because they were abolished by the mutation of a conserved arginine residue in the CNBD to glutamate (R591E) (Figures 5B and 5C). This mutation was previously shown to abolish the facilitatory effect of cAMP on wild-type HCN and CNG subunits by causing a 2000-fold decrease in the sensitivity of the channel to cAMP (Chen et al., 2001; Tibbs et al., 1998).

The FPN Tripeptide Reverses the Normal Action of cAMP to Promote Tetramerization of the HCN2 C-Linker + CNBD Polypeptide

To obtain insight into the structural mechanism by which the C-linker tripeptide controls the polarity of ligand gating, we examined the oligomeric assembly in free solution of the HCN2 C-terminal polypeptide (consisting of the C-linker + CNBD) whose crystal structure had been solved (Zagotta et al., 2003). In this previous study,

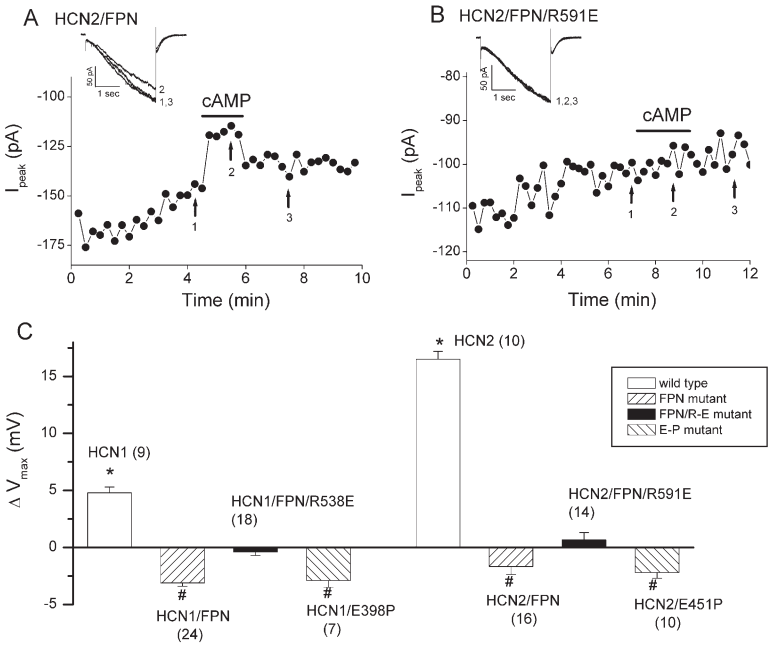

Figure 5. Properties of Inverse Agonist Effects of cAMP on HCN2 Mutant Channels

(A) cAMP produced a rapid and reversible inhibition of HCN2/FPN. Circles plot peak currents at end of 3 s steps to −100 mV during the experiment. Inserts show currents in response to steps to −100 mV before (1), during (2), and after (3) 10 μM cAMP application.

(B) cAMP has no effect on HCN2/FPN/R591E mutant channels. Currents elicited by step to −100 mV. (Inset) Currents in presence and absence of cAMP superimpose.

(C) Summary of mean effects of cAMP on tail current activation curves of HCN1 and HCN2 wild-type and mutant channels. ΔV_{max} is maximal shift in $V_{1/2}$ with saturating cAMP. Numbers of experiments are indicated in parentheses. HCN1/E398P and HCN2/E451P are single point mutants with an exchange of only the middle residue of FPN/QEK tripeptides. Other labels are defined in text. *Voltage shift with cAMP was significantly greater than zero (positive shift) ($p < 0.01$). #Effect of cAMP was significantly less than zero (negative shift) ($p < 0.01$ for HCN1/FPN; $p < 0.04$ for HCN2/FPN). cAMP (10 μM) had no significant effect on the $V_{1/2}$ of HCN1/FPN/R538E ($p = 0.15$) or HCN2/FPN/R591E ($p = 0.36$). $V_{1/2}$ values in the absence of cAMP were −100.1 ± 1.1 mV ($n = 18$) for HCN1/FPN/R538E and −118.5 ± 1.8 mV ($n = 11$) for HCN2/FPN/R591E.

analytical ultracentrifugation was also used to determine the effects of cAMP binding on the state of oligomerization of the C-terminal polypeptide in free solution. These experiments showed that in the absence of cAMP the polypeptide existed largely as a monomer, with some dimer present (Zagotta et al., 2003); cAMP binding greatly enhanced the concentration of tetramers and decreased the concentration of dimers. This suggested the hypothesis that it is the formation of the tetrameric gating ring upon cAMP binding that enhances channel opening. Our finding that the FPN mutation both facilitated HCN channel opening in the absence of cAMP and converted cAMP into an inverse agonist led us to predict that the FPN mutant C-terminal domain should show an increased tendency to form tetramers in the absence of cAMP and that such tetramers should be disassembled upon cAMP binding.

To test these predictions, we performed analytical ultracentrifugation studies on the HCN2/FPN polypeptide in free solution (Figures 6A and 6B). In the absence of cAMP, the FPN mutant polypeptide did indeed form a significant amount of the tetrameric species, with relatively little dimer present. This is in contrast to the behavior of the wild-type polypeptide, where there is little tetramer but a significant amount of dimer and monomer present in the absence of ligand. Importantly, we found that application of cAMP to the mutant polypeptide now *decreased* the amount of tetramer and *enhanced* the amount of dimer that was present, the opposite to the effects previously observed for wild-type HCN2.

Based on a simple monomer to dimer to tetramer model, we derived association constants for the oligomerization reaction. Cyclic AMP binding to the wild-type HCN2 polypeptide normally increased the association constant for the assembly of two wild-type dimers into a tetramer, K_{24}, by 660-fold (Figures 6C and 6D). In contrast, cAMP binding *decreased* this association constant in the FPN mutant by ~4-fold (Figures 6E and 6F). These biochemical results thus paralleled the effects of the mutation to reverse the polarity of cAMP gating, supporting the view that a transition in the oligomerization state of C-terminal domains to a 4-fold symmetric gating ring is part of the fundamental mechanism that underlies ligand gating.

Discussion

Our results show that a C-linker tripeptide that regulates differences in agonist efficacy between CNG channel α and β subunits also has a marked effect on ligand gating in HCN subunits, indicating a conservation of the fundamental mechanism of ligand gating between the two major classes of cyclic nucleotide-regulated channels. We further found that the efficacy of ligand gating was diminished when the fCNGA4 FPN tripeptide was incorporated in heteromeric CNG channels. Surprisingly, when the FPN tripeptide of fCNGA4 subunits was substituted for the native tripeptide of HCN subunits (QEK), the polarity of action of cAMP was switched from that of an agonist to that of an inverse agonist.

At present, we cannot determine whether the FPN sequence also switches the polarity of ligand gating in CNG channels, because CNG subunits containing this sequence fail to express as functional homomers. Furthermore, although the FPN sequence is clearly an important reason why CNGA4 fails to form functional cyclic nucleotide-gated channels, other C-linker CNGA4 sequences also contribute to preventing functional homo-

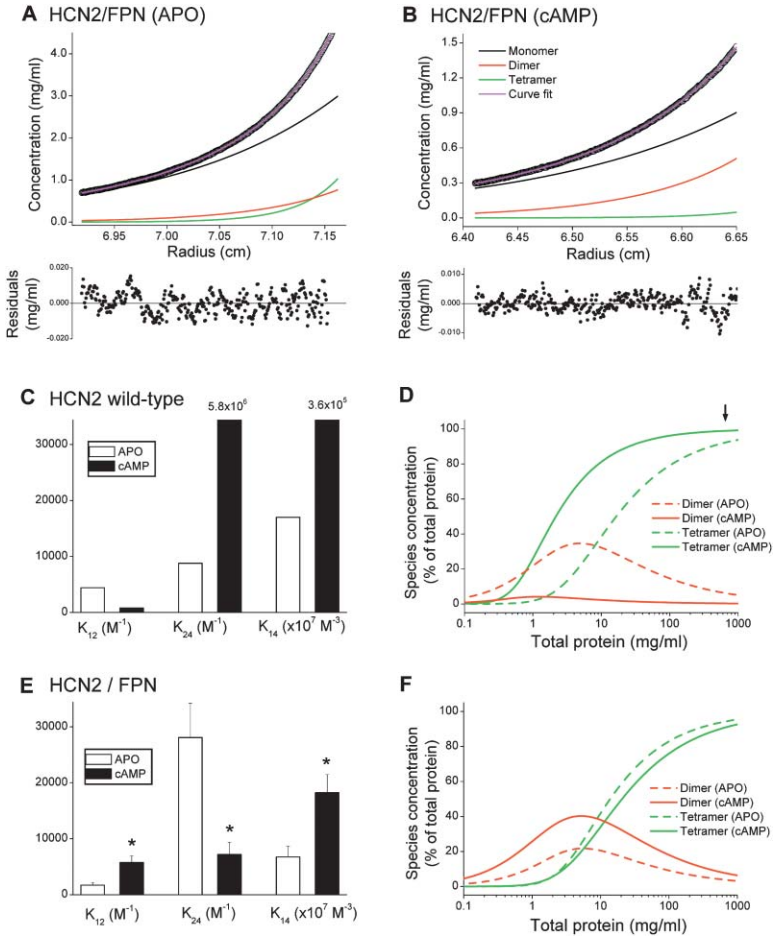

Figure 6. HCN2/FPN Mutation Reverses the Effect of cAMP on Oligomerization of a Soluble C-Terminal HCN2 Polypeptide

(A and B) Protein concentration distribution curves from analytical ultracentrifugation of HCN2/FPN protein in the absence ([A]; Apo state) and in the presence of 5 mM cAMP (B) after reaching sedimentation equilibrium at 17,000 rpm. A three-species model (monomer, black; dimer, red; tetramer, green) was used to fit the raw data (purple). The corresponding residuals of the curve fit are at bottom.

(C) Self-association constants for wild-type HCN2I protein: K_{12} (monomer-dimer), K_{24} (dimer-tetramer), and K_{14} (monomer-tetramer). The values for K_{24} and K_{14} in presence of cAMP are off-scale and shown at top. For the apo state, the average association constants are as follows: K_{12}, 4400 M^{-1}; K_{24}, 8781 M^{-1}; K_{14}, 1.7×10^{11} M^{-3}. For the cAMP bound state, the association constants are as follows: K_{12}, 764 M^{-1}; K_{24}, 5.8×10^{6} M^{-1}; K_{14}, 3.4×10^{12} M^{-3}. Data and values in (C) taken from Zagotta et al., 2003. Arrow shows protein concentration used for crystal structure.

(D) Calculated mass percentage of dimer (red) or tetramer (green) as a function of total HCN2I concentration. Total protein was calculated as $[\text{monomer}] + 2 \times K_{12} \times [\text{monomer}]^2 + 4 \times K_{14} \times [\text{monomer}]^4$. Monomer traces are not shown.

(E) Self-association constants for HCN2/FPN protein. Error bars represent SEM. For apo state: K_{12}, 1694 ± 460 M^{-1}; K_{24}, $28{,}081 \pm 6{,}129$ M^{-1}; K_{14}, $6.75 \pm 1.90 \times 10^{10}$ M^{-3} ($n = 4$). For cAMP bound state: K_{12}, 5729 ± 1240 M^{-1}; K_{24}, 7182 ± 2176 M^{-1}; K_{14}, $18.2 \pm 3.2 \times 10^{10}$ M^{-3}. Asterisk indicates significant difference between cAMP bound state and apo state ($p < 0.03$).

(F) Percentage of dimer (red) or tetramer (green) plotted as a function of total HCN2/FPN concentration.

mer expression, since the simple replacement of the CNGA4 FPN sequence with the QAR α subunit sequence was not sufficient to yield functional channels. Moreover, CNGB1 and CNGB3 β subunits, which also fail to form functional homomers, do not contain the FPN sequence, again indicating that additional regions of CNG β subunits act to suppress functional expression of homomeric channels.

The low efficacy of cyclic nucleotide activation of heteromeric channels containing the CNGA4 subunit raises the interesting question as to what evolutionary advantage such weak gating could confer on the CNG channels of olfactory neurons that incorporate this subunit. A potential rationale is provided by our finding that the voltage-dependent gating of α + β heteromers vanished at high concentrations of ligand when the FPN tripeptide of the β subunit was replaced by the QAR tripeptide of the α subunit. Our results further showed that this effect of the QAR tripeptide is due to the high efficacy of the resultant heteromeric channels ($P_{max} \approx 1$), which occludes the ability of depolarization to enhance macroscopic CNG current at saturating concentrations of cyclic nucleotide. Thus, we suggest that the reduced efficacy of α + β heteromers serves to enhance the ability of regulatory signals, such as membrane depolarization, to modulate the gating of CNG channels. A very high efficacy will also limit the extent to which small inhibitory energetic perturbations, such as that due to Ca^{2+}/calmodulin binding (Bradley et al., 2001; Munger et al., 2001), can depress CNG currents at saturating concentrations of cyclic nucleotide. In this manner, the C-linker tripeptide of the fCNGA4 subunit may tune the gating of a heteromeric CNG channel to respond to a variety of physiological signals. However, because olfactory CNG channels contain two α subunits and one each of CNGA4 and CNGB1 (Bonigk et al., 1999; Sautter et al., 1998; Zheng and Zagotta, 2004), the precise nature of the energetic contribution of CNGA4 to a native channel will require further investigation.

What are the structural changes that underlie the ability of the QXR/K:FPN tripeptides to act as a gating switch? According to the HCN2 crystal structure, the tripeptide is located in the middle of the first, or A′, α helix of the C-linker (Figure 7A), near the last (S6) transmembrane segment. The A′-B′ helix pair normally interacts with the C′-D′ helix pair in the C-linker of a

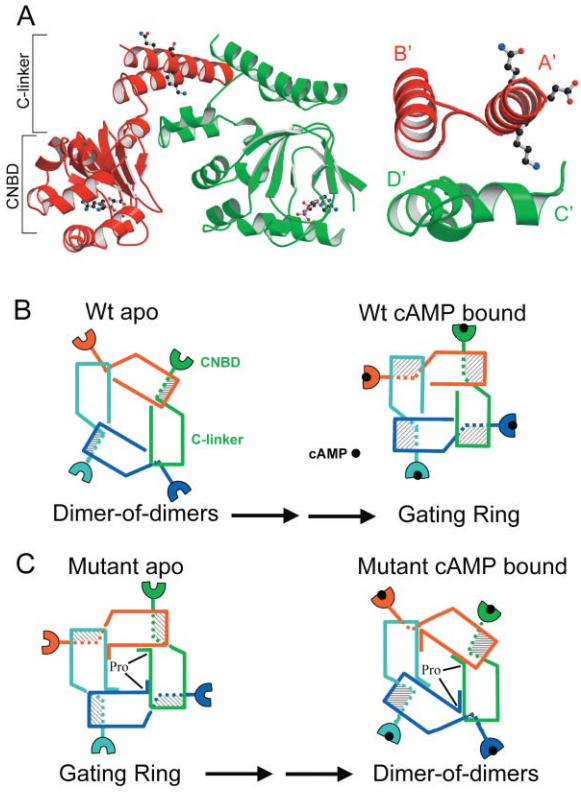

Figure 7. Model for Regulation of Channel Gating by Cyclic Nucleotide-Induced Change in Oligomerization State between C-Terminal Ligand Gating Domains

(A) Wild-type subunit interface between two neighboring HCN2 C-terminal polypeptide protomers (shown in red and green) in a 4-fold symmetric tetramer. (Left) Approximate positions of A′–F′ helices of the C-linker and C-terminal CNBD are indicated. Bound cAMP molecules are indicated as ball and stick figures in the CNBDs. The view is perpendicular to the 4-fold axis in the center of the molecule. A zoom-in view of the C-linker intersubunit interface shows the A′ and B′ helices of one subunit (red) contacting the C′ and D′ helices of a neighboring subunit (green). Ball and stick figures show location of the side chains for the wild-type QEK residues in the A′ helix of the red protomer. (Coordinates from Zagotta et al., 2003.)

(B and C) Model for change in C-terminal oligomerization symmetry during cyclic nucleotide gating for wild-type and FPN mutant HCN channels. In wild-type channels (B), the four C-linker + CNBD (labeled for one subunit) domains are shown to associate as a dimer-of-dimers with 2-fold symmetry in the absence of cyclic nucleotide (apo). The C-terminal regions of each subunit are shown in a different color. The blue and cyan subunits constitute one dimer; the green and red subunits constitute the second dimer. Note the asymmetry between subunit interfaces within a dimer versus between two dimers. Strength of interaction at each interface is indicated by dashed area of subunit-subunit overlap. Cyclic nucleotide binding promotes independent conformational changes in each dimer to an active state. When both dimers have activated, assembly of a 4-fold symmetric gating ring occurs that enhances channel activation. In FPN mutant channels (C), we propose that there is an increased tendency for the 4-fold symmetric gating ring to form in the absence of cAMP, due to a proline-induced kink (Pro) in the A′ helix. This accounts for the enhanced activation (positive shift in $V_{1/2}$) in the absence of cAMP of FPN mutant channels relative to wild-type channels. cAMP binding favors the dimer-of-dimers state of oligomerization in mutant channels, which inhibits their opening by hyperpolarization.

neighboring subunit, providing the major intersubunit contacts that mediate gating ring assembly. The first two residues of QEK face away from the interior of the structure and thus cannot be important for C-linker intersubunit interactions; they may interact with the nearby transmembrane domain that is not present in the crystal structure. Although lysine 452 of QEK does point toward residues in the C′ helix, it is not essential, because a K452A point mutant shows normal ligand gating (data not shown). Thus, the switch in gating is most likely due to the introduction of a kink in the A′ helix by the proline residue in the FPN tripeptide. Indeed, we found that the E451P point mutation in HCN2 is sufficient to reverse the polarity of cAMP gating (Figure 5C). However, in CNG channels the flanking residues do play some role, since the single proline to alanine mutation in fCNGA4 failed to enhance gating to the same extent as did the FPN to QAR triple mutation (data not shown).

Based on the finding that cAMP binding promotes gating ring formation in wild-type HCN2, we propose that this binding event normally alters the orientation of the C′-D′ helixes of one subunit relative to the A′-B′ helixes of a neighboring other subunit to form a complementary interface that enables assembly of a 4-fold symmetric gating ring (Figure 7B). In the absence of cAMP, the subunits would adopt an orientation that favors the 2-fold symmetry of a dimer-of-dimers, in which a subunit pair within a dimer forms a stronger interface compared to the interface between the two dimers. Introduction of a proline bend in the A′ helix would alter this relationship so that the 4-fold symmetric interface now becomes more favored in the absence of ligand than in its presence; conversely, the 2-fold symmetric dimeric interface becomes more favorable in the presence of cAMP than in its absence. As a result, ligand binding to the mutant channel will enhance gating ring disassembly (Figure 7C).

The correlation that we found between the effect of the FPN sequence on the polarity of agonist gating and the polarity of C-terminal assembly provides strong evidence that ligand gating involves the dynamic assembly and disassembly of the 4-fold symmetric gating ring from a dimer-of-dimers. Formation of the gating ring is proposed to facilitate channel opening, consistent with the correlation that we find between conditions that enhance gating ring assembly (i.e., presence of cAMP in wild-type HCN2 versus absence of cAMP in the HCN2/FPN mutant) and the ease of HCN channel activation by hyperpolarization. A cyclic nucleotide-dependent transition from a dimer-of-dimers into a 4-fold symmetric gating ring is also consistent with a reaction scheme based on the functional stoichiometry and subunit cooperativity of cyclic nucleotide gating for both CNG (Liu et al., 1998; Liu et al., 1996) and HCN (Ulens and Siegelbaum, 2003) channels. Given the presence of tetrameric and dimeric assemblies in a large number of channels, the dynamic oligomerization of C-terminal ligand binding domains may prove to be a general mechanism underlying ligand gating.

Experimental Procedures

Molecular Biology

A cDNA library was constructed from catfish olfactory epithelium mRNA and inserted into a λ-gt10 expression vector (Goulding et al.,

1992). *CNGA4* clones were isolated using degenerate primers based on the rat *CNGA4* sequence to amplify a highly conserved region in CNG channels (S5 to the β3-strand in the CNBD) from the catfish cDNA library. The PCR product was used to make a ^{32}P-labeled DNA probe to screen the library. XL1-Blue MRF competent cells (Stratagene; #200302) were used as the host, and 10^6 plaque-forming units were plated out in the first round. Plaques were lifted and transferred to Hybond-N nylon membrane (Amersham). Hybridization was carried out in Express Hyb hybridization solution (Clontech; #8015-2) at 50°C for 2 hr followed by washing with 0.5× SSC. Positive cDNA clones encoding full-length *fCNGA4* were isolated and subcloned into the pGEM-HE vector (Liman and Buck, 1994). 3′UTRs and 5′UTRs were removed by PCR. The cDNA sequence has been deposited in GenBank (AF522297).

Chimeras were constructed using the "megaprimer" strategy. The sequence to be exchanged was amplified with chimeric primers (usually >50 bp), which covered the junction region of both parental constructs. This PCR product was used as a new primer (megaprimer) to amplify the target construct. A Quickchange kit was used to introduce point mutations. mRNA was synthesized using mMessage mMachine Kit (Ambion; #1340).

ROONS is a high-expressing chimera of purely α subunit sequence, consisting of bCNGA1 whose P region and an amino terminal region (N-S2) were replaced by fCNGA2 α subunit sequence, as previously described (Goulding et al., 1994; Tibbs et al., 1997, 1998).

Electrophysiology

Xenopus oocytes were injected with 5–100 ng cRNA for the various constructs, and recordings were obtained 2–9 days after injection, as previously described (Goulding et al., 1992). Inside-out patches were obtained, and currents were recorded with an EPC-9 amplifier (Heka), with 1–3 MΩ patch pipettes. The bath solution and pipette solution were symmetrical and contained 67 mM KCl, 30 mM NaCl, 10 mM HEPES, 10 mM EGTA, and 1 mM EDTA (pH 7.4). All data were filtered at 5 kHz and digitized at 20 kHz. Experiments were performed at room temperature (22°C–24°C). KK peptide (MAAVAGLYGLGKKRQHRKKQ) is the Shaker K^+ channel inactivation ball peptide with two lysine substitutions (Kramer et al., 1994; Murrell-Lagnado and Aldrich, 1993) and was synthesized by the protein chemistry core facility of Columbia University.

For HCN channels, 50 ng of cRNA was injected into each oocyte, which were studied 2–3 days after injection. Inside-out patches were superfused with bath solution for 4–5 min before experiments. Bath solution and pipette solution were symmetrical and contained 107 mM KCl, 5 mM NaCl, 10 mM HEPES, 1 mM $MgCl_2$, and 1 mM EGTA (pH 7.4) (Wang et al., 2001). Currents were recorded in response to a series of 3 s hyperpolarizing voltage steps, starting at −70 mV down to a maximal negative value of −140 mV to −160 mV, in 10 mV increments. The maximal negative voltage was chosen so that the tail current approached its maximal value. This voltage varied depending on the particular construct and experimental conditions. Tail currents were measured upon return to the holding potential of −40 mV and normalized to the maximal tail current following the most negative voltage step. Due to rundown of HCN currents, tail currents were measured before cAMP application (4–5 min after obtaining the patch), in the presence of cAMP (1–2 min after application), and after removal of cAMP (1–2 min after washout). The tail currents from the two measurements in the absence of cAMP were averaged. Tail current activation curves were fitted by a Boltzmann function as previously described to obtain the midpoint voltage of activation ($V_{1/2}$) (Wainger et al., 2001). The effect of cAMP was measured as the difference between $V_{1/2}$ values in the presence and absence of cAMP ($\Delta V_{1/2}$).

Open-Channel Block Model

Channel kinetics in the presence of saturating concentrations of cAMP (1 mM) and 10 μM KK peptide were simulated with a three-state model:

$$C \underset{\beta}{\overset{\alpha}{\rightleftharpoons}} O + B \underset{k_b}{\overset{k_f}{\rightleftharpoons}} OB \qquad (1)$$

where C is the closed state, O is the open state, B is KK peptide, and OB is the open-blocked state. α and β are voltage- and ligand-dependent rate constants for channel opening and closing, respectively. k_f and k_b are forward and reverse rate constants for peptide binding and unbinding, respectively. Tail currents (following voltage step from +100 mV to −140 mV) with KK peptide present were fitted with the sum of two exponential functions (time constants τ_1 and τ_2):

$$O(t) = O_\infty + A \cdot e^{-\frac{t}{\tau_1}} + B \cdot e^{-\frac{t}{\tau_2}} \qquad (2)$$

We then derived estimates for channel open probability, P_O, in the absence of KK peptide from the additional following measurements and equations. We measured the time course of channel deactivation in the absence of KK peptide using a single exponential function (time constant, τ'). Steady-state currents were measured at the hyperpolarized test potentials elicited by a saturating concentration of cAMP in the presence (O_∞) or absence (O'_∞) of KK peptide, where [KK] is the concentration of KK peptide applied (10 μM). We then obtained O_T, the maximal current if all channels were open, by solving the following equations:

$$P_O = \frac{O'_\infty}{O_T} = \frac{\alpha}{\alpha + \beta} \qquad (3)$$

$$\tau' = \frac{1}{\alpha + \beta} \qquad (4)$$

$$O_T = O_\infty \cdot \left(1 + \frac{\beta}{\alpha} + \frac{[KK] \cdot k_f}{k_b}\right) \qquad (5)$$

$$\frac{1}{\tau_1} + \frac{1}{\tau_2} = \alpha + \beta + [KK] \cdot k_f + k_b \qquad (6)$$

$$\frac{1}{\tau_1 \cdot \tau_2} = \alpha \cdot k_b + \alpha \cdot [KK] \cdot k_f + \beta \cdot k_b \qquad (7)$$

Protein Purification and Sedimentation Equilibrium Assay

Soluble His-tagged HCN2I/FPN constructs were expressed in bacterial BL-21 cells as described (Zagotta et al., 2003). Bacteria were collected and resuspended in lysis buffer (30 mM HEPES, 300 mM NaCl, 5% sucrose, 1 mM β-mercaptoethanol, 0.1 mM phenylmethylsulphonyl chloride, and 2.5 μg ml^{-1} DNase [pH 7.5]). The supernatant from a 45 min, 120,000 g spin was loaded onto Ni^{2+}-NTA column. His-tagged HCN2/FPN was eluted by imidazole with a linear concentration gradient (from 50 mM to 400 mM). Following thrombinolysis (reaction buffer contained 20 mM HEPES, 300 mM NaCl, 5% sucrose, 5 mM $CaCl_2$, and 1 mM dithiothreitol [pH 7.0]) to remove the His tag, the protein was loaded onto an S-sepharose ion exchange column and eluted with a linear NaCl gradient (100 mM–500 mM).

Protein was purified by size exclusion chromatography and concentrated to 3–4 mg ml^{-1}, split into two pools, and dialyzed against buffer (20 mM HEPES, 300 mM NaCl, 1 mM dithiothreitol, and 5% sucrose [pH 7]) with or without 5 mM cAMP. Centrifugation experiments were repeated four times with loaded protein concentrations diluted using protein:buffer ratios of 1:0, 1:1, or 1:3. Sedimentation equilibrium runs were conducted in an XL-I analytical ultracentrifuge (Beckman/Coulter) with the Rayleigh interference detection system. The protein samples with and without cAMP were loaded into two- or six-sector centrifugation cells and centrifuged at 4°C at 12,000, 17,000, and 25,000 rpm. Scans were taken at 1 hr intervals until the samples reached equilibrium. Data were edited with WinReedit and globally fitted by a nonlinear least-squares method to a three-species model (monomer, dimer, and tetramer) with WinNONLIN (http://spin6.mcb.uconn.edu/winnonlin/winnonln.html). Reduced molecular weight was calculated with SEDNTERP (http://www.jphilo.mailway.com/svedberg.htm). The self-association constant between dimer and tetramer (K_{24}) was calculated as $K_{14}/(K_{12})^2$.

Acknowledgments

We thank Gareth Tibbs, Leslie Vosshall, and Zhong-Ping Sun for help in the cloning of fCNGA4; and Eric Gouaux for his generous help and advice with the AUC experiments. We thank Damian Bell, Chris Ulens, and Brian Wainger for their helpful comments on the

manuscript. Finally, we thank John Riley for expert technical assistance; Len Zablow for help with modeling; and Satinder Singh for help with the AUC experiments. N.B.O. was supported by a NIH training grant in Molecular Biophysics. Funding for the analytical ultracentrifuge was provided by the NIH. This work was partially supported by grant NS36658 from NIH (to S.A.S.).

Received: July 29, 2004
Revised: September 28, 2004
Accepted: November 3, 2004
Published: December 1, 2004

References

Altomare, C., Terragni, B., Brioschi, C., Milanesi, R., Pagliuca, C., Viscomi, C., Moroni, A., Baruscotti, M., and DiFrancesco, D. (2003). Heteromeric HCN1–HCN4 channels: a comparison with native pacemaker channels from the rabbit sinoatrial node. J. Physiol. *549*, 347–359.

Bonigk, W., Bradley, J., Muller, F., Sesti, F., Boekhoff, I., Ronnett, G.V., Kaupp, U.B., and Frings, S. (1999). The native rat olfactory cyclic nucleotide-gated channel is composed of three distinct subunits. J. Neurosci. *19*, 5332–5347.

Bradley, J., Li, J., Davidson, N., Lester, H.A., and Zinn, K. (1994). Heteromeric olfactory cyclic nucleotide-gated channels: a subunit that confers increased sensitivity to cAMP. Proc. Natl. Acad. Sci. USA *91*, 8890–8894.

Bradley, J., Reuter, D., and Frings, S. (2001). Facilitation of calmodulin-mediated odor adaptation by cAMP-gated channel subunits. Science *294*, 2176–2178.

Broillet, M.C., and Firestein, S. (1997). β subunits of the olfactory cyclic nucleotide-gated channel form a nitric oxide activated Ca^{2+} channel. Neuron *18*, 951–958.

Bucossi, G., Nizzari, M., and Torre, V. (1997). Single-channel properties of ionic channels gated by cyclic nucleotides. Biophys. J. *72*, 1165–1181.

Chen, S., Wang, J., and Siegelbaum, S.A. (2001). Properties of hyperpolarization-activated pacemaker current defined by coassembly of HCN1 and HCN2 subunits and basal modulation by cyclic nucleotide. J. Gen. Physiol. *117*, 491–504.

Cheng, K.T., Chan, F.L., Huang, Y., Chan, W.Y., and Yao, X. (2003). Expression of olfactory-type cyclic nucleotide-gated channel (CNGA2) in vascular tissues. Histochem. Cell Biol. *120*, 475–481.

Dhallan, R.S., Yau, K.W., Schrader, K.A., and Reed, R.R. (1990). Primary structure and functional expression of a cyclic nucleotide-activated channel from olfactory neurons. Nature *347*, 184–187.

Gerstner, A., Zong, X., Hofmann, F., and Biel, M. (2000). Molecular cloning and functional characterization of a new modulatory cyclic nucleotide-gated channel subunit from mouse retina. J. Neurosci. *20*, 1324–1332.

Goulding, E.H., Ngai, J., Kramer, R.H., Colicos, S., Axel, R., Siegelbaum, S.A., and Chess, A. (1992). Molecular cloning and single-channel properties of the cyclic nucleotide-gated channel from catfish olfactory neurons. Neuron *8*, 45–58.

Goulding, E.H., Tibbs, G.R., and Siegelbaum, S.A. (1994). Molecular mechanism of cyclic-nucleotide-gated channel activation. Nature *372*, 369–374.

Higgins, M.K., Weitz, D., Warne, T., Schertler, G.F., and Kaupp, U.B. (2002). Molecular architecture of a retinal cGMP-gated channel: the arrangement of the cytoplasmic domains. EMBO J. *21*, 2087–2094.

Jiang, Y., Lee, A., Chen, J., Cadene, M., Chait, B.T., and MacKinnon, R. (2002). Crystal structure and mechanism of a calcium-gated potassium channel. Nature *417*, 515–522.

Johnson, J.P., Jr., and Zagotta, W.N. (2001). Rotational movement during cyclic nucleotide-gated channel opening. Nature *412*, 917–921.

Karpen, J.W. (1997). Why do cyclic nucleotide-gated channels have the jitters? Biophys. J. *72*, 986–988.

Karpen, J.W., Zimmerman, A.L., Stryer, L., and Baylor, D.A. (1988). Gating kinetics of the cyclic-GMP-activated channel of retinal rods: flash photolysis and voltage-jump studies. Proc. Natl. Acad. Sci. USA *85*, 1287–1291.

Kaupp, U.B., and Seifert, R. (2002). Cyclic nucleotide-gated ion channels. Physiol. Rev. *82*, 769–824.

Kaupp, U.B., Niidome, T., Tanabe, T., Terada, S., Bonigk, W., Stuhmer, W., Cook, N.J., Kangawa, K., Matsuo, H., Hirose, T., et al. (1989). Primary structure and functional expression from complementary DNA of the rod photoreceptor cyclic GMP-gated channel. Nature *342*, 762–766.

Kramer, R.H., Goulding, E., and Siegelbaum, S.A. (1994). Potassium channel inactivation peptide blocks cyclic nucleotide-gated channels by binding to the conserved pore domain. Neuron *12*, 655–662.

Kuo, A., Gulbis, J.M., Antcliff, J.F., Rahman, T., Lowe, E.D., Zimmer, J., Cuthbertson, J., Ashcroft, F.M., Ezaki, T., and Doyle, D.A. (2003). Crystal structure of the potassium channel KirBac1.1 in the closed state. Science *300*, 1922–1926.

Liman, E.R., and Buck, L.B. (1994). A second subunit of the olfactory cyclic nucleotide-gated channel confers high sensitivity to cAMP. Neuron *13*, 611–621.

Liu, D.T., Tibbs, G.R., and Siegelbaum, S.A. (1996). Subunit stoichiometry of cyclic nucleotide-gated channels and effects of subunit order on channel function. Neuron *16*, 983–990.

Liu, D.T., Tibbs, G.R., Paoletti, P., and Siegelbaum, S.A. (1998). Constraining ligand-binding site stoichiometry suggests that a cyclic nucleotide-gated channel is composed of two functional dimers. Neuron *21*, 235–248.

Matulef, K., and Zagotta, W.N. (2003). Cyclic nucleotide-gated ion channels. Annu. Rev. Cell Dev. Biol. *19*, 23–44.

Much, B., Wahl-Schott, C., Zong, X., Schneider, A., Baumann, L., Moosmang, S., Ludwig, A., and Biel, M. (2003). Role of subunit heteromerization and N-linked glycosylation in the formation of functional hyperpolarization-activated cyclic nucleotide-gated channels. J. Biol. Chem. *278*, 43781–43786.

Munger, S.D., Lane, A.P., Zhong, H., Leinders-Zufall, T., Yau, K.W., Zufall, F., and Reed, R.R. (2001). Central role of the CNGA4 channel subunit in Ca2+-calmodulin-dependent odor adaptation. Science *294*, 2172–2175.

Murrell-Lagnado, R.D., and Aldrich, R.W. (1993). Energetics of Shaker K channels block by inactivation peptides. J. Gen. Physiol. *102*, 977–1003.

Paoletti, P., Young, E.C., and Siegelbaum, S.A. (1999). C-Linker of cyclic nucleotide-gated channels controls coupling of ligand binding to channel gating. J. Gen. Physiol. *113*, 17–34.

Peng, C., Rich, E.D., and Varnum, M.D. (2004). Subunit configuration of heteromeric cone cyclic nucleotide-gated channels. Neuron *42*, 401–410.

Robinson, R.B., and Siegelbaum, S.A. (2003). Hyperpolarization-activated cation currents: from molecules to physiological function. Annu. Rev. Physiol. *65*, 453–480.

Sautter, A., Zong, X., Hofmann, F., and Biel, M. (1998). An isoform of the rod photoreceptor cyclic nucleotide-gated channel β subunit expressed in olfactory neurons. Proc. Natl. Acad. Sci. USA *95*, 4696–4701.

Schumacher, M.A., Rivard, A.F., Bachinger, H.P., and Adelman, J.P. (2001). Structure of the gating domain of a Ca2+-activated K+ channel complexed with Ca2+/calmodulin. Nature *410*, 1120–1124.

Scott, S.P., Weber, I.T., Harrison, R.W., Carey, J., and Tanaka, J.C. (2001). A functioning chimera of the cyclic nucleotide-binding domain from the bovine retinal rod ion channel and the DNA-binding domain from catabolite gene-activating protein. Biochemistry *40*, 7464–7473.

Sun, Y., Olson, R., Horning, M., Armstrong, N., Mayer, M., and Gouaux, E. (2002). Mechanism of glutamate receptor desensitization. Nature *417*, 245–253.

Tibbs, G.R., Goulding, E.H., and Siegelbaum, S.A. (1997). Allosteric activation and tuning of ligand efficacy in cyclic-nucleotide-gated channels. Nature *386*, 612–615.

Tibbs, G.R., Liu, D.T., Leypold, B.G., and Siegelbaum, S.A. (1998). A state-independent interaction between ligand and a conserved

arginine residue in cyclic nucleotide-gated channels reveals a functional polarity of the cyclic nucleotide binding site. J. Biol. Chem. *273*, 4497–4505.

Ulens, C., and Siegelbaum, S.A. (2003). Regulation of hyperpolarization-activated HCN channels by cAMP through a gating switch in binding domain symmetry. Neuron *40*, 959–970.

Ulens, C., and Tytgat, J. (2001). Functional heteromerization of HCN1 and HCN2 pacemaker channels. J. Biol. Chem. *276*, 6069–6072.

Wainger, B.J., DeGennaro, M., Santoro, B., Siegelbaum, S.A., and Tibbs, G.R. (2001). Molecular mechanism of cAMP modulation of HCN pacemaker channels. Nature *411*, 805–810.

Wang, J., Chen, S., and Siegelbaum, S.A. (2001). Regulation of hyperpolarization-activated HCN channel gating and cAMP modulation due to interactions of COOH terminus and core transmembrane regions. J. Gen. Physiol. *118*, 237–250.

Weitz, D., Ficek, N., Kremmer, E., Bauer, P.J., and Kaupp, U.B. (2002). Subunit stoichiometry of the CNG channel of rod photoreceptors. Neuron *36*, 881–889.

Weyand, I., Godde, M., Frings, S., Weiner, J., Muller, F., Altenhofen, W., Hatt, H., and Kaupp, U.B. (1994). Cloning and functional expression of a cyclic-nucleotide-gated channel from mammalian sperm. Nature *368*, 859–863.

Young, E.C., Sciubba, D.M., and Siegelbaum, S.A. (2001). Efficient coupling of ligand binding to channel opening by the binding domain of a modulatory (β) subunit of the olfactory cyclic nucleotide-gated channel. J. Gen. Physiol. *118*, 523–546.

Zagotta, W.N., and Siegelbaum, S.A. (1996). Structure and function of cyclic nucleotide-gated channels. Annu. Rev. Neurosci. *19*, 235–263.

Zagotta, W.N., Olivier, N.B., Black, K.D., Young, E.C., Olson, R., and Gouaux, E. (2003). Structural basis for modulation and agonist specificity of HCN pacemaker channels. Nature *425*, 200–205.

Zheng, J., and Zagotta, W.N. (2004). Stoichiometry and assembly of olfactory cyclic nucleotide-gated channels. Neuron *42*, 411–421.

Zheng, J., Trudeau, M.C., and Zagotta, W.N. (2002). Rod cyclic nucleotide-gated channels have a stoichiometry of three CNGA1 subunits and one CNGB1 subunit. Neuron *36*, 891–896.

Zhong, H., Molday, L.L., Molday, R.S., and Yau, K.W. (2002). The heteromeric cyclic nucleotide-gated channel adopts a 3A:1B stoichiometry. Nature *420*, 193–198.

Zhou, W., Qian, Y., Kunjilwar, K., Pfaffinger, P.J., and Choe, S. (2004). Structural insights into the functional interaction of KChIP1 with Shal-type K(+) channels. Neuron *41*, 573–586.

Zong, X., Zucker, H., Hofmann, F., and Biel, M. (1998). Three amino acids in the C-linker are major determinants of gating in cyclic nucleotide-gated channels. EMBO J. *17*, 353–362.

Accession Numbers

The GenBank accession number for the *CNGA4* cDNA sequence reported in this paper is AF522297.